

Science Meets Technology with Advanced Optical Metrology

Access in-depth information on methods and applications in the R&D field of optical metrology through free to access article digests of recent peer-reviewed publications and more.

Discover advancedopticalmetrology.com now!

OLYMPUS

WILEY

Energy Harvesting from Breeze Wind (0.7–6 m s⁻¹) Using Ultra-Stretchable Triboelectric Nanogenerator

Zewei Ren, Ziming Wang, Zhirong Liu, Longfei Wang, Hengyu Guo, Linlin Li, Site Li, Xiangyu Chen,* Wei Tang,* and Zhong Lin Wang*

Wind is one of the most important sources of green energy, but the current technology for harvesting wind energy is only effective when the wind speed is beyond 3.5–4.0 m s⁻¹. This is mainly due to the limitation that the electromagnetic generator works best at high frequency. This means that light breezes cannot reach the wind velocity threshold of current wind turbines. Here, a high-performance triboelectric nanogenerator (TEENG) for efficiently harvesting energy from an ambient gentle wind, especially for speeds below 3 m s⁻¹ is reported, by taking advantage of the relative high efficiency of TENGs at low-frequency. Attributed to the multiplied-frequency vibration of ultra-stretchable and perforated electrodes, an average output of 20 mW m⁻³ can be achieved with inlet wind speed of 0.7 m s⁻¹, while an average energy conversion efficiency of 7.8% at wind speed of 2.5 m s⁻¹ is reached. A self-charging power package is developed and the applicability of the TENG in various light breezes is demonstrated. This work demonstrates the advantages of TENG technology for breeze energy exploitation and proposes an effective supplementary approach for current employed wind turbines and micro energy structure.

1. Introduction

Wind energy has played an essential role in global green energy since it is plentiful, renewable, and widespread.^[1,2] Many large wind farms are established since the wind turbine technology has been extensively studied. The capacity installed worldwide is cumulative up to 591 GW by the end of 2018.^[3] Megawatts of power can be generated merely by a single wind turbine as it operates under optimized conditions.^[4–6] However, a technological shortcoming existed in these machines is that the wind speed should be more than 3 m s⁻¹ (their manufactured cut-in speed, usually 3.5–4.0 m s⁻¹ on modern turbines^[7]) in order to generate power to the utility system,^[8–12] as limited by the physics of the electromagnetic generator.^[13,14] Nevertheless, the most of the wind available in the environment is low-speed airflows, which is below the turbines' threshold speed.^[15,16] The ubiquitously

distributed light breeze would be an effective micro energy source for current small portable electronic devices and Internet of things (IoTs). Since the light breeze energy can't be harvested by the conventional turbines effectively,^[17,18] this part of energy has been wasted in vain. Meanwhile, the harvesting of light breeze energy is generally regarded limited may attribute to the unsatisfactory efficiency of these conventional energy scavengers under low-speed wind. The device with high efficiency under low-speed wind is urgently necessary, to propose a significant approach for current energy harvesting of light breeze.

Recently, the invention of the triboelectric nanogenerator (TEENG) has offered an unprecedented approach for efficiently converting environmental agitations into high electric outputs,^[19,20] especially for energy resources within low mechanical frequency, such as wind, rain drop, and water wave.^[21–24] Accordingly, a series of TENG prototypes have been investigated targeting at wind energy harvesting, where various novel architectures and materials are applied.^[25–27] However, these reports are focused on scavenging high-speed wind energy (>5 m s⁻¹), and the light breeze energy harvesting by these devices is infeasible since minimum operating speed thresholds of these devices are still rather high.^[28–33] To collect energy

Dr. Z. Ren, Dr. Z. Wang, Dr. Z. Liu, Dr. L. Wang, Prof. L. Li, Prof. X. Chen, Prof. W. Tang, Prof. Z. L. Wang
CAS Center for Excellence in Nanoscience
Beijing Key Laboratory of Micro-nano Energy and Sensor
Beijing Institute of Nanoenergy and Nanosystems
Chinese Academy of Sciences
Beijing 100083, China
E-mail: chenxiangyu@binn.cas.cn; tangwei@binn.cas.cn; zhong.wang@mse.gatech.edu

Dr. Z. Ren, Dr. Z. Wang, Dr. Z. Liu, Prof. L. Li, Prof. X. Chen, Prof. W. Tang, Prof. Z. L. Wang
School of Nanoscience and Technology
University of Chinese Academy of Sciences
Beijing 100049, China

Dr. L. Wang, Dr. H. Guo, Prof. Z. L. Wang
School of Material Science and Engineering
Georgia Institute of Technology
Atlanta, GA 30332-0245, USA

Dr. S. Li
Department of Chemistry
Carnegie Mellon University
Pittsburgh, PA 15213, USA

 The ORCID identification number(s) for the author(s) of this article can be found under <https://doi.org/10.1002/aenm.202001770>.

DOI: 10.1002/aenm.202001770

from low-frequency excitation of gentle wind, material and architecture of the entire device need to be systematically optimized to acquire multiplied-frequency output.

Here, we demonstrated that a gentle wind-driven TENG (GW-TENG) can efficiently harvest energy from ultralow-speed wind/airflow ($0.7\text{--}6\text{ m s}^{-1}$). Different from previously reported generators for gentle wind energy harvesting, the GW-TENG utilizes the ultra-stretchable, perforated film electrode that resembles a stirred rubber band when driven by gentle flow, to acquire an effective output from multiplied-frequency vibration. An average power density of 20 mW m^{-3} can be achieved with inlet wind speed of 0.7 m s^{-1} , while an average energy conversion efficiency of 7.8% at wind speed of 2.5 m s^{-1} has been reached, indicating the superiority of GW-TENG for low-speed airflow energy harvesting. Coupling with the self-charging power package, the GW-TENG has been exhibited as direct power supply for wireless transmission, toward the trend of next-generation TENG serving

wearable electronics and IoTs. The applicability of GW-TENG has been demonstrated in situations of gentle wind induced by the fan of a working laptop, turning pages of a book and the side-road air flow created by a passing car. This work proposed an effective strategy to harvest ubiquitously distributed but usually neglected low-speed airflows and gentle intermittent wind source, which is of great importance and can be an effective supplement for current micro energy structure.

2. Results and Discussion

2.1. Design and Operation of GW-TENG

A schematic of GW-TENG for gentle wind energy harvesting is shown in **Figure 1a**. The velocity comparison and corresponding visible natural phenomena for the proposed gentle wind/breeze are shown in Table S1 (Supporting Information).

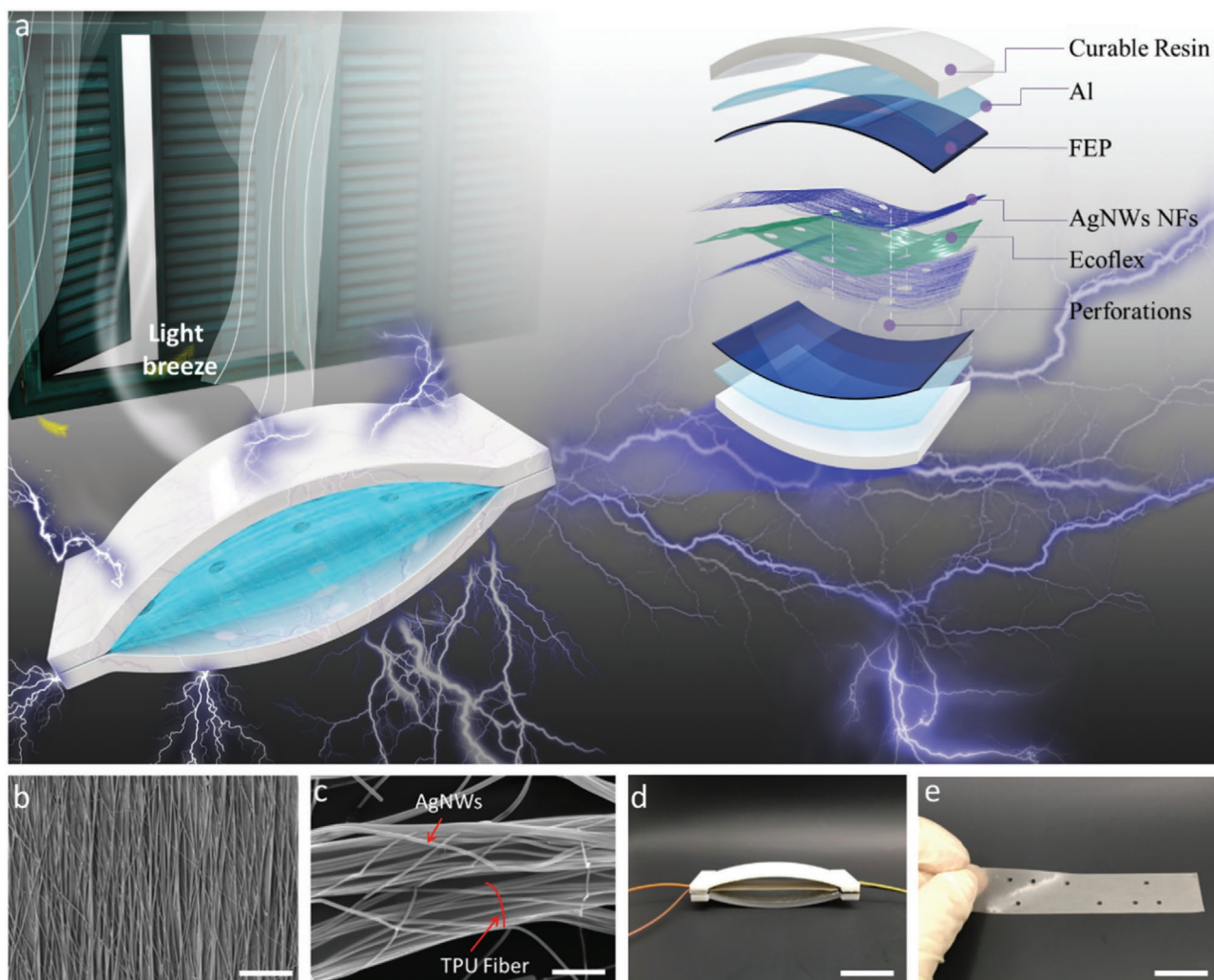


Figure 1. Structure design of the GW-TENG. a) Schematic diagram of GW-TENG for light breeze energy harvesting. Insets: Partially enlarged diagram of AgNW NFs. b) SEM image of unidirectional TPU NFs. Scale bar: $50\text{ }\mu\text{m}$. c) Micromorphology of the AgNW NFs, where TPU NF is wrapped by long-distance ordered AgNWs cluster. Scale bar: 600 nm . d) Photograph of the GW-TENG. Scale bar: 3 cm . e) Photograph of the ultra-stretchable AgNW NFs film electrode. Scale bar: 22 mm .

The structure of GW-TENG can be divided into three parts: arch-shaped frameworks, negative tribo-layer, and ultra-stretchable film electrode sandwiched in them (inset in Figure 1a). The arched components are made by 3D printing with UV curable resin. Fluorinated ethylene propylene (FEP) is chosen as dielectric material of GW-TENG, whose surface has been treated by plasma etching for introducing nanostructures (Figure S1a, Supporting Information) to enhance the tribo charge density. The unidirectional thermoplastic polyurethanes (TPU) spinning nanofibers (NFs) modified by ultra-long silver nanowires (AgNWs) has been compounded on surfaces of the ultra-thin Ecoflex substrate, functioning as the positive electrode tribo-layer. Scanning electron microscopy (SEM) images and photographs of TPU NFs mesh before conductive treatment by AgNWs are shown in Figure 1b and Figure S1b–d (Supporting Information). The TPU NFs wrapped by long-distance ordered AgNWs cluster are prepared (Figure 1c and Figure S1e, Supporting Information) by dilute AgNWs transfer using a unidirectional glass grating frame. The adhesion between the NFs and AgNWs would be adequately strong, due to the NF surfaces would be slightly corrode by the *N,N*-dimethylacetamide that added to the dilute AgNWs solution. The Ecoflex substrate is obtained by spin-coating and the prepared AgNW NFs are attached to the substrate surface to form a semi-embedded structure, before the substrate is completely cured. This semi-embedded structure can ensure good extensibility and surface conductivity of the electrode. Meanwhile, the ravine-like surface microstructure (atomic force microscopy image in Figure S1f, Supporting Information) formed by these semi-embedded conducting NFs on the electrode is crucial for enhancing the output of GW-TENG. Because electrostatic induction can be greatly enhanced by this ravine-like microstructure with “occlusion effect,” which has been reported by a latest research.^[34] The whole GW-TENG device presents an “arch” shape (Figure 1d) to increase triboelectric area between the elastic electrode and FEP layer, the design principle of which is presented in Note S1 (Supporting Information). To further improve the aeroelastic effect of the ultra-stretchable elastic electrode and enhance the electrode’s vibration performance, the distributed perforations have been introduced on the electrode. Since the perforations on the film can create prescribed inhomogeneous flow profiles and thus enhance the aeroelastic effect.^[35] The electrode sandwiched in the GW-TENG would integrate two TENG units in one device, realizing the maximized space utilization, as photographs and schematics exhibited in Figure 1d and Figure S4 (Supporting Information).

The working principle of GW-TENG for breeze energy harvesting can be elucidated from two aspects: Namely, wind flow deforms elastic electrode, and electrode deformation generates electric output. When the middle film electrode deforms and vibrates in the airflow, the alternating output can be induced in the external circuit, ascribed to continuous contact-electrification and electrostatic-induction between this elastic electrode and FEP dielectric layer^[36] (the details can be found in Figure S5a, Supporting Information). The potential distribution under the open-circuit condition is simulated, as depicted in Figure S5b (Supporting Information).

2.2. Material Design and Optimization for the Ultra-Stretchable Electrode

For conversion into electricity of low-speed wind through GW-TENG efficiently, the material component and physical (mechanical and electrical) properties of the gentle flow-driven electrode are essential, requiring it to be stretchable, elastic, and light in weight. Figure 2a,b shows the tensile property of unidirectional TPU NFs mesh. It is noteworthy that with the mesh thickness near 10 μm, elongation of the NFs mesh can reach 400% before broken, indicating a satisfied mechanical property for fabrication of the electrode. For the substrate film of the electrode, the mechanical behavior of which ought to resemble a plucked rubber band when driven by breeze, to acquire multiplied-frequency contact-separate motion from low-frequency excitation of gentle wind. That’s because a positive correlation between the output of TENG device and frequency of contact-separate motion exists,^[37] and an adequate vibration amplitude of the motional electrode is also necessary to ensure sufficient contact-separate distance,^[38] based on the equations:

$$I_{sc} = \frac{2S\sigma d_0 x_{max} f}{(d_0 + x(t))^2} \quad (1)$$

$$\overline{P_{opt}} \propto f \text{ or } \overline{P_{opt}} = \text{Log}_{10} f + D \quad (2)$$

where I_{sc} is the absolute short-circuit current of TENG, S is the size of contact area, σ is the triboelectric surface charge density, f is triggering frequency of mechanical energy, $x(t)$ is real-time contact-separate distance (x_{max} is the maximum), d_0 is the effective thickness of the dielectric layer defined as $d_0 = \sum d_i/\epsilon_i$,^[36] $\overline{P_{opt}}$ is the optimized average output power of TENG, D is a constant.

$$V_{oc} = -\frac{Q}{S\epsilon_0} \cdot (d_0 + x(t)) + \frac{\sigma x(t)}{\epsilon_0} \quad (3)$$

V_{oc} is open-circuit voltage of TENG, Q is transferred charges between the two tribo-layers, and ϵ_0 is permittivity of vacuum. The detailed derivation of Equations (1)–(3) can be found in Note S2 (Supporting Information). To clearly demonstrate that in experiment, flow-induced vibrations of several ultrathin films of distinct materials were studied under wind flow of 2 m s⁻¹, in which their vibration amplitude and frequency are shown in Figure S6 and Video 1 (Supporting Information). The performance of silicon rubber is more desirable, that is, the characteristic of which in low-speed air flow ought to like the behavior of a plucked rubber band or bowstring. Only in this way, multiplied-frequency of contact-separate motion can be acquired from the low-frequency excitation of gentle flow, and the efficiency of energy acquisition can be improved. In this case, Ecoflex 00-50 has ultimately been a reasonable choice as substrate material of the electrode. The elastic modulus of the pure Ecoflex substrate film and the compound electrode are shown in Figure 2c. The Ecoflex 00-50 films used there have not been treated with pre-tension. In addition, the geometric parameters (length, width, thickness) of the electrode have been investigated systematically, with ultimate optimized dimension

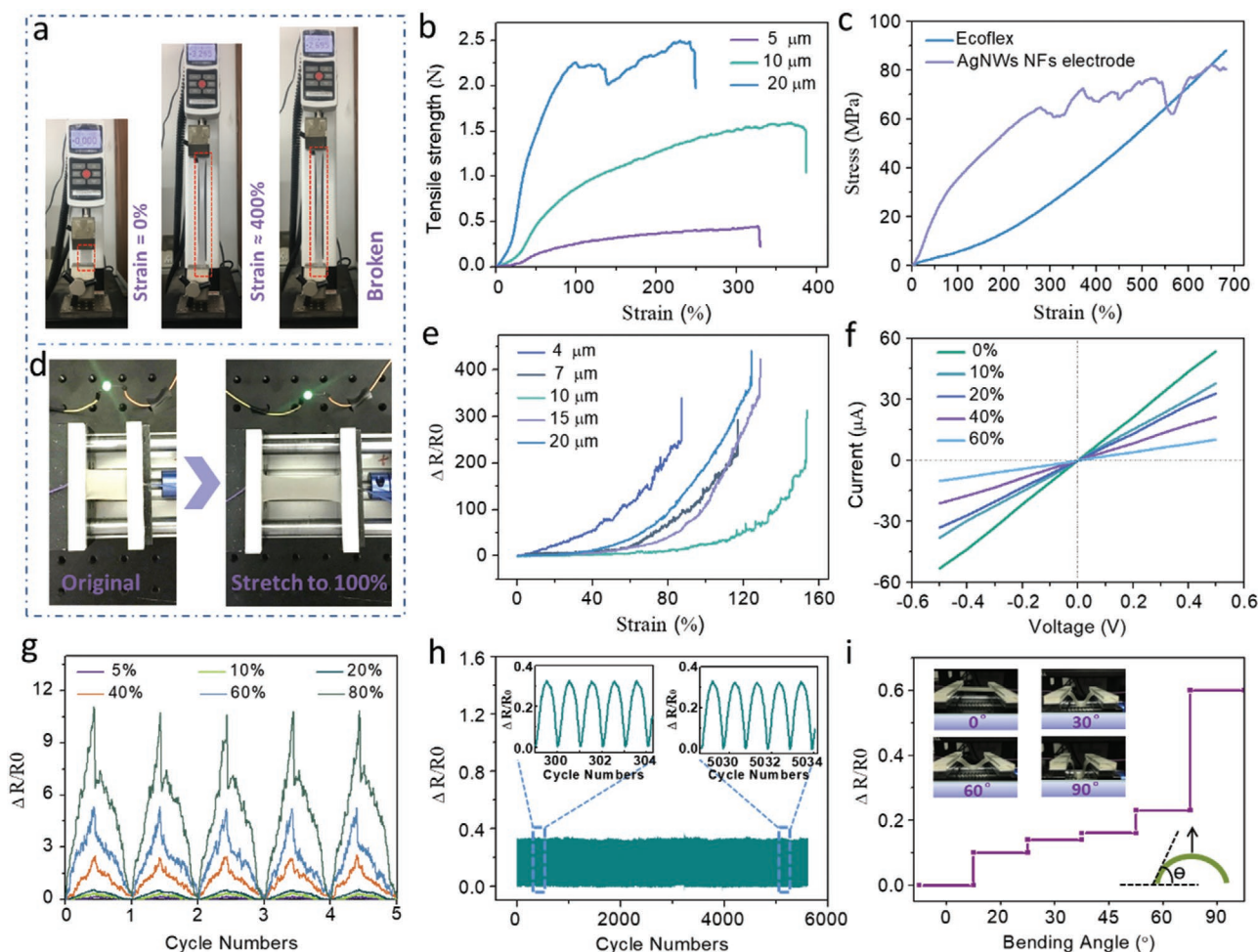


Figure 2. Mechanical behavior and electrical conductivity of the AgNW NFs electrode. a) The TPU NFs mesh at initial state (0% strain) and stretched state (400% strain). b) Elastic properties of TPU NFs mesh with distinct thickness. c) Tensile test of the compound electrode based on Ecoflex substrate and AgNW NFs mesh (10 μm). d) Photographs of the electrode connected in the LED circuit when tensile strain changing from 0% to 100%. e) $\Delta R/R_0$ of the electrode versus tensile strain ε with AgNW NF meshes in different thickness. f) Current–voltage curves of the electrode at different strains. g) Multi-cycle tests of $\Delta R/R_0$ change of the electrode when stretched to different maximum strains. h) Stability test of AgNW NFs electrode with maximum strain of 10% for around 6000 cycles. i) Conductivity change of the electrode in the bending deformation.

of 8 cm \times 2 cm \times 120 μm . The details are shown in Figure S7 and Note S3 (Supporting Information).

Figure 2e illustrates a relative change in resistance ($\Delta R/R_0$) of the electrode, in which thicknesses of the compounded AgNW NFs mesh are various. With thickness of 10 μm , the AgNW NFs electrode can withstand strain up to about 160%. Obviously, the stretchability of the electrode can be precisely modulated by further modifying density and size of AgNW NFs. Figure 2f demonstrates current–voltage curves of the electrode under different strains. Photographs of the electrode connected to a green light-emitting diode (LED) circuit when the strain changing from 0% to 100% are shown in Figure 2d. Aiming for practical applications, the conductive stretching stability and durability of AgNW NFs electrode are studied. Multi-cycle tests for $\Delta R/R_0$ of the electrode when it's stretched to different strains are carried out (Figure 2g), where the tested electrode shows a stable cyclic behavior. The fatigue durability of this AgNW NFs electrode is also tested with a strain of 10% for about 6000 cycles, during which the variation of $\Delta R/R_0$

exhibits good repeatability (Figure 2h). The conductivity of the electrode stands in bending deformation is also illustrated, as shown in Figure 2i. These results imply that AgNW NFs film electrode is satisfactory for the fabrication of GW-TENG, with both reliable mechanical and electrical properties.

2.3. Performance of GW-TENG

Performance of GW-TENG for breeze energy harvesting is demonstrated in Figure 3. A closed-loop wind tunnel control system is constructed to precisely control the inlet wind speed for standardized tests (Figure 3a). The uniformity of the flow in the testing tunnel has been demonstrated by measuring flow velocity of nine featured points (inset of Figure 3a and Figure S8, Supporting Information). Figure 3b illustrates the dependence of output (V_{oc} and I_{sc}) of GW-TENG on the airflow, ranging from 0.7 to 6.0 m s^{-1} (the outputs there in Figure 3 come from a unit of GW-TENG). It's noted that the V_{oc} and I_{sc} increase

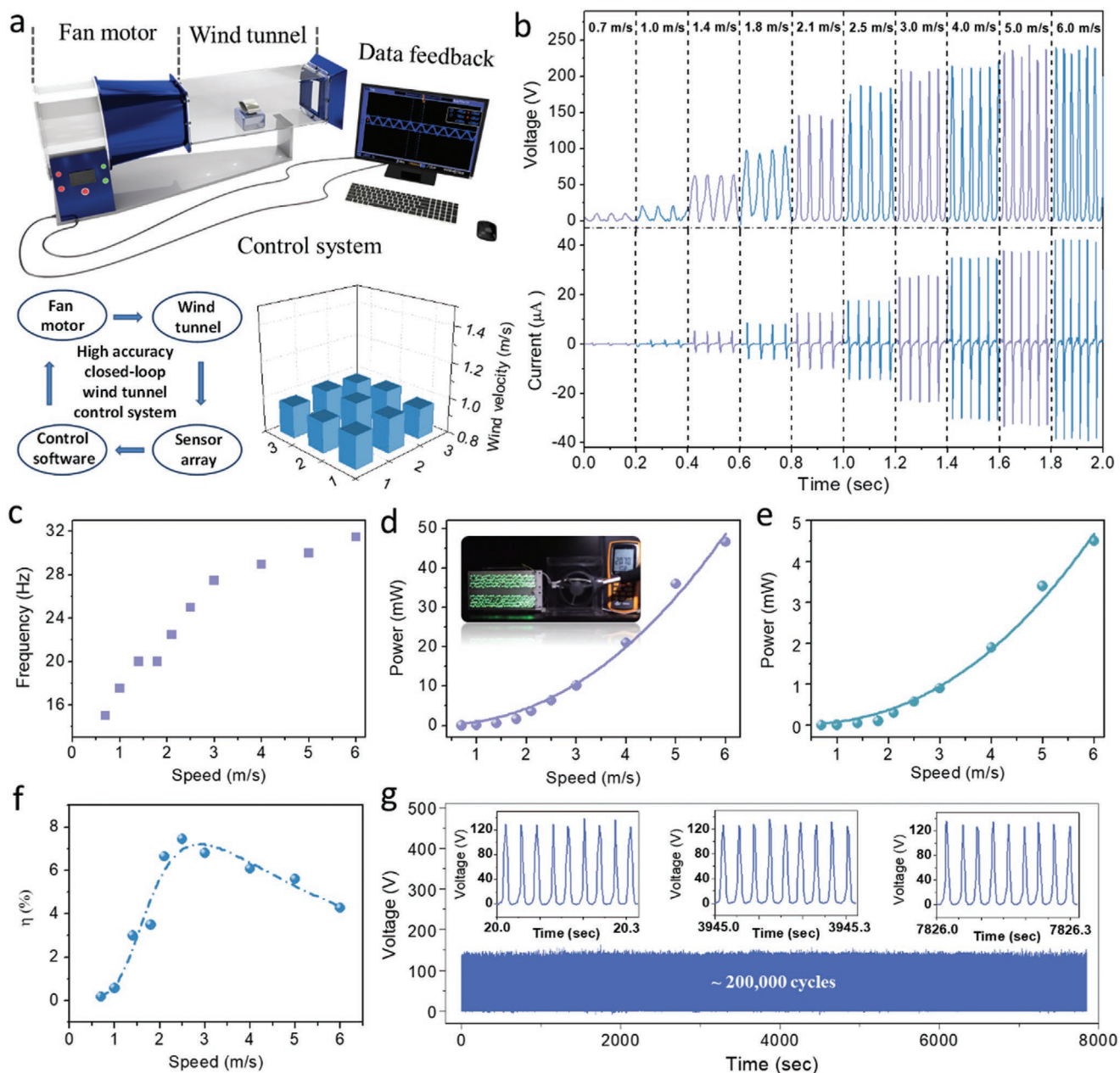


Figure 3. Electrical characteristics of GW-TENG. a) The self-feedback wind tunnel control system with closed loop circuit for output testing of GW-TENG. Insets: the closed loop circuit and the smoothness test of the generated airflow in the tunnel. b) Dependence of V_{oc} and I_{sc} induced by GW-TENG with the airflow velocity ranging from 0.7 to 6.0 m s^{-1} . c) The changing motion frequency of the AgNW NFs electrode corresponding to the increasing flow velocity. d) The instantaneous output power and e) average power of GW-TENG in the air flow. f) Average energy conversion efficiency of GW-TENG. g) Durability test of output of GW-TENG with continuous working cycles around 200 000.

near linearly with the flow velocity until 3 m s^{-1} , beyond which the peak value trends gently. The phenomenon results from two aspects: saturation of contact area between AgNW NFs film electrode and the negative layer; vibration frequency changing of AgNW NFs electrode (Figure 3c). This change can attribute to the relationship between lift force and elastic restoring force of AgNW NFs electrode. Figure 3d,e illustrates the instantaneous and average output power of GW-TENG, respectively. The corresponding load-output curves are depicted in Figure S9 (Supporting Information). Furthermore, both surface

and volumetric power density of GW-TENG are calculated. To grasp the latest researches of scavengers for gentle wind energy harvesting, we have collected the literatures and made a systematic comparison of these existed devices, as details shown in Tables S2 and S3 (Supporting Information). An average power density of 0.4 and 20 mW m^{-3} can be achieved by GW-TENG with inlet wind speed of 0.7 m s^{-1} . The output power density of GW-TENG reported here is so far the highest one to the best of our knowledge, under the certain same flow velocity ($<6 \text{ m s}^{-1}$). The result illustrates the superiority of this GW-TENG device

based on TENG technology in low-frequency energy harvesting, comparing to the electromagnetic and piezoelectric generators. The comparison detail is demonstrated in Note S4 (Supporting Information). The prominent output of GW-TENG is also directly elaborated by lighting 240 LEDs simultaneously even the wind speed is merely 2 m s^{-1} (Video S2, Supporting Information).

Figure 3f demonstrates the average energy conversion efficiency η of GW-TENG for harvesting light breeze energy, where η is defined as the ratio of generated electricity by GW-TENG W_g and inlet wind energy E_k ,

$$\eta = \frac{W_g}{E_k} \quad (4)$$

which can be further expressed as:

$$\eta = \frac{2 \int_0^T I_{sc}^2 R dt}{\int_0^T \rho S [U(t)]^3 dt} \quad (5)$$

R is the internal impedance of GW-TENG, ρ is the air density, S is air-inlet area, and $U(t)$ is the inlet wind speed. The detailed derivation can be found in Note S5 (Supporting Information). As Figure 3f shown, the η changes with inlet-wind intensity and the superiority of this GW-TENG for low flow energy harvesting is demonstrated, in which the η reaches maximum of 78% at inlet wind speed of 2.5 m s . Besides, the durability of GW-TENG is tested with continuous working cycles of around 200 000, where the output of GW-TENG performs stable with no apparent fluctuation (Figure 3g).

2.4. Self-Charging Power Package and the Applicability of GW-TENG

To utilize the generated electricity from GW-TENG more effectively, a self-charging power package is developed based on a modified power management circuit, as shown in Figure 4a. The circuit of the energy package is presented in Figure 4f, where the core modules include power energy transfer, self-management energy storage, and DC buck conversion. To improve the performance of the energy storage, the polyester-film capacitor instead of previous Al electrolyte capacitors^[39,40] is adopted there with almost no leakage (Figure 4b). Figure 4c presents charging curves of this polyester-film and other two Al-electrolyte capacitors (100 V, 50 μF), charged by the same TENG (Figure S10, Supporting Information), in which charging property of the polyester-film capacitor is always linear and stable up to its rated voltage. Here, the electric energy from GW-TENG can be autonomously storage, modulated to steady DC output and supply to the external load by this energy package. Therefore, this self-charging power package can be a power supply for small electronic equipment and information transmission. The long-distance wireless transmission based on this energy package as energy source has been demonstrated, as shown in Figure 4g and Video S3 (Supporting Information). After the energy package with capacitance of 100 μF is charged for about 2 min by three paralleled GW-TENGs (with gentle wind

of 2 m s^{-1}). The wireless transmitter (Figure 4d) is powered to emit a trigger signal to remotely switch a red warning light in the receiver (Figure 4e). The voltage variation of the energy package for two consequent transmitting processes can be found in Figure 4h.

Since gentle wind ubiquitously exists in various ambient situations, the GW-TENG can be widely applicable as energy harvester or power supply for sensing systems. Here, the applicability of GW-TENG in three breeze situations is demonstrated, to be specific, gentle airflow induced by the fan of a working laptop, turning pages of a book and the road-side air flow created by a passing car, as depicted in Figure 5a. For a majority of electrical equipment, recycling the wind energy of their cooling fans may be an alternative approach to save the limited energy supply. As presented in Figure 5b and Video S4 (Supporting Information), the gentle wind induced by cooling fan of the working laptop can be effectively harvested by GW-TENG. The generated electricity can directly power a display board with 120 LEDs. Meanwhile, the output signal can be a sensing source for detection of the machine's working state. In Figure 5c and Video S4 (Supporting Information), the gentle intermittent wind source resulting from turning pages of a notebook is effectively collected by GW-TENG. The generated electrical signal of which is shown in Figure 5e. Besides, the energy harvesting of air flow at the roadside induced by the passing cars is worthy attention, since a huge energy demand of numerous road-side equipment exist. Figure 5d,f and Video S5 (Supporting Information) have elaborated the feasibility of this energy collecting by GW-TENG. Here, the passing car has a lateral distance of 2 m to GW-TENG, significantly beyond the standard safe distance to the roadside (usually 0.6 m). Thus, when a large number of GW-TENGs are set at side of roads with huge traffic flows, the collected energy can be considerable. Besides, the self-powered traffic monitoring system based on GW-TENG is also potentially demonstrated, as the distinct output signals in Figure 5f shown. When running speed of the passing car is low ($<20 \text{ km h}^{-1}$), there is no electricity generated from GW-TENG since the induced air flow is too weak to operate the device (Video S5, Supporting Information). With the speed increases, obvious output signals can be acquired, and accordingly, amplitude and duration time of the signal would be enhanced (Figure 5f). Overall, these explorations validate the extensive practical applicability of GW-TENG in our ambient situations. Meanwhile, for practical application, some protective means can be taken to guarantee the effectivity of GW-TENG for energy harvesting of natural breeze wind, the details are demonstrated in Figure S21 (Supporting Information).

3. Conclusion

In summary, we have demonstrated a high-performance strategy to efficiently harvest breeze energy based on TENG technology. Different from the previous reported generators, the GW-TENG utilize the ultra-stretchable, perforated electrode that resembles a stirred rubber band when driven by gentle flow, to acquire effective output from multiplied-frequency vibration. An average power density of 20 mW m^{-3} can be achieved with inlet wind speed of 0.7 m s^{-1} , and an average energy conversion

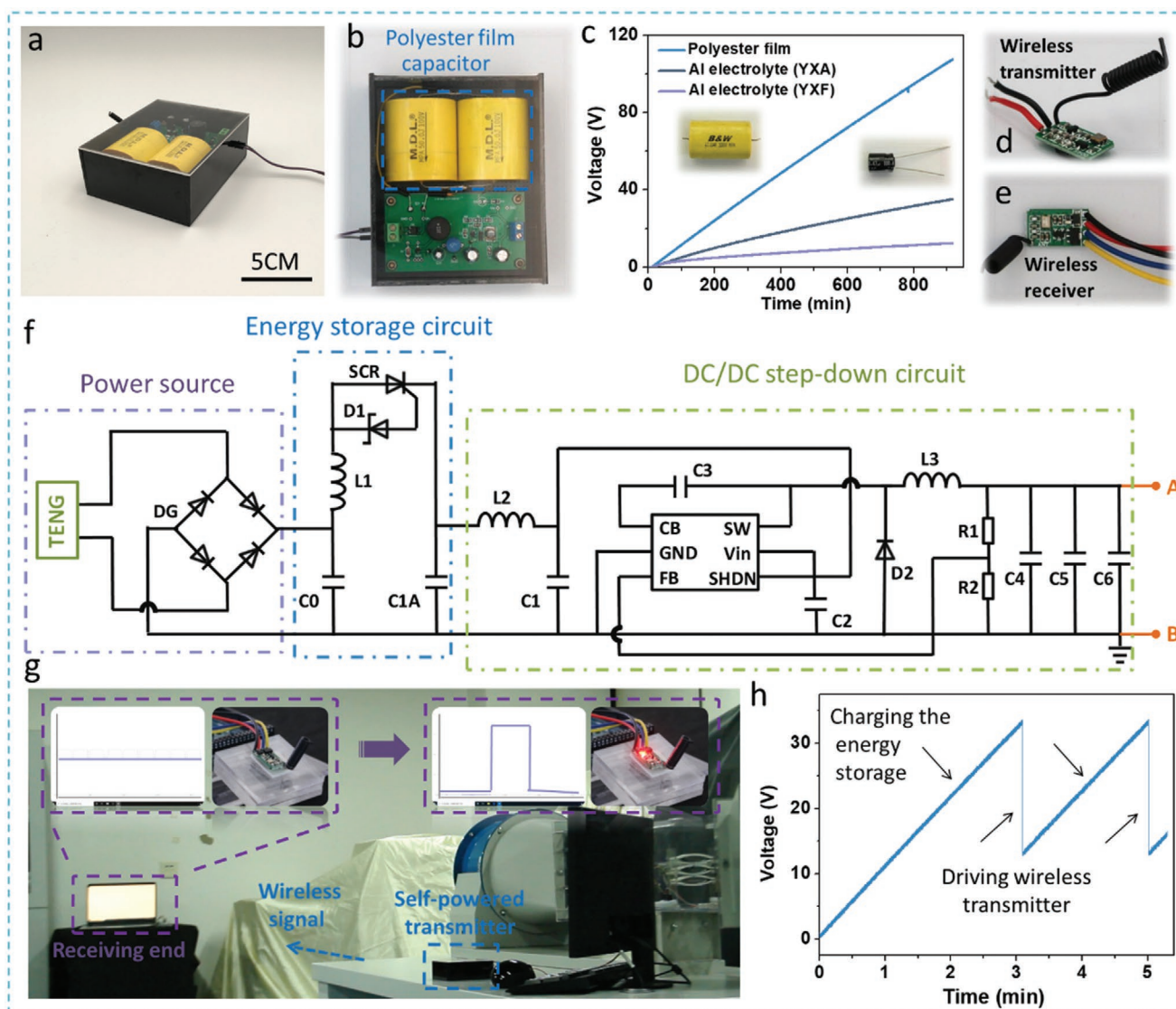


Figure 4. Illustration of the self-charging energy package. a,b) Photographs of the energy package and polyester-film capacitor. c) Charging curves of the polyester-film and several Al-electrolyte capacitors (100 V, 50 μ F). d,e) Photographs of the wireless transmitter and receiver. f) Circuit schematic of the energy package. g) Demonstration of the energy package as an effective energy supply for long-distance wireless transmission. h) Voltage variation of the energy package in two consequent transmitting processes.

efficiency of 7.8% at inlet speed of 2.5 m s^{-1} has been reached, indicating the superiority of GW-TENG for low-speed airflow energy harvesting. The average output power density within the low-speed range ($0.7\text{--}6 \text{ m s}^{-1}$) is the highest among its peers to the best of our knowledge. To utilize the generated electricity from GW-TENG more effectively, a self-charging power package is developed based on a modified power management circuit. The integrated self-powered micro energy system has been exhibited as directly power supply for wireless transmission, toward the trend of next-generation TENG serving wearable electronics and IoTs. Light breeze is ubiquitous in ambient situations, the applicability of GW-TENG has been demonstrated via gentle wind induced by the fan of a working laptop, turning pages of a book or the road-side airflow created by a passing car, and etc. Our study establishes a novel approach for

efficiently scavenging commonly neglected low-speed breeze, and may function as a feasible supplementary strategy for current employed wind turbines and micro energy structure.

4. Experimental Section

Fabrication of Ultra-Thin, Ultra-Stretchable AgNW NFs Electrode: The unidirectional TPU NFs mesh was prepared using electrospinning (Shenzhen Tong Li Tech Co. Ltd.). TPU spinning solution was poured into a plastic syringe with a blunted G10 needle and a constant potential (10 kV) was adopted between the needle and the grounded metal collectors. The AgNWs were transferred from the dilute solution (with 0.5% *N,N*-dimethylacetamide, by volume) to TPU NFs mesh by a unidirectional glass grating frame, with transfer of several times to acquire the AgNW NFs. The diameter of AgNW was 50 nm with length

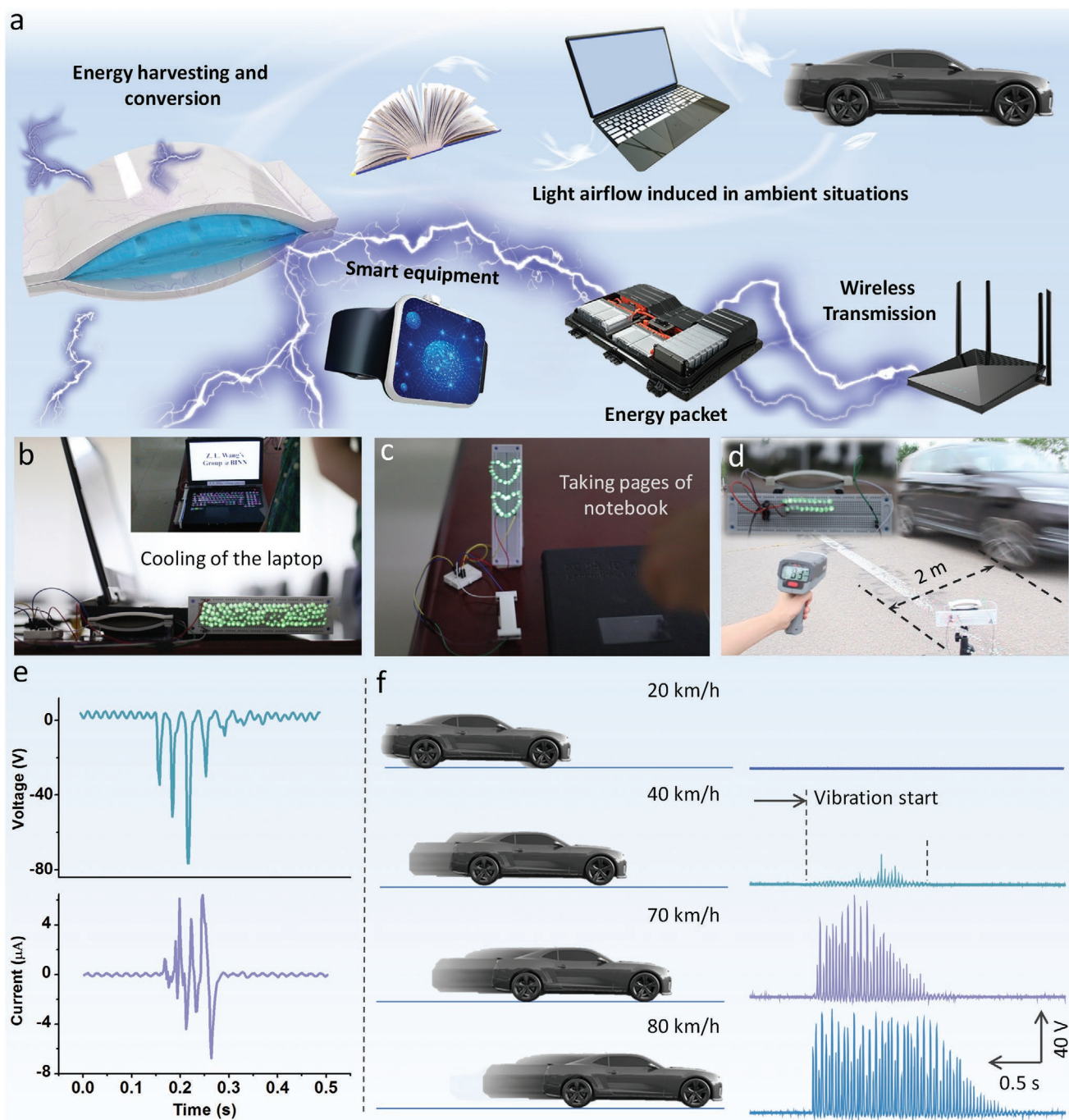


Figure 5. Illustration of the applicability of GW-TENG. a) Schematic of the applicability of GW-TENG in ambient various situations. Energy harvesting from b) light breeze induced by a working laptop, c) gentle intermittent wind induced by turning over pages of a notebook, or d) air flow at the roadside created by a passing car. e) Output signal of the GW-TENG for gentle wind harvesting induced by turning over pages of a notebook. f) Schematic and distinct output signals from GW-TENG when the car passes with different running speed.

of 100–200 μm , which was purchased from XFNANO Tech, China. The Ecoflex film substrate (around 100 μm) was obtained by spin-coating (500 r min^{-1}), with Ecoflex solution mixed by parts A and B (1:1 by mass), and then cured at vacuum chamber with 40 $^{\circ}\text{C}$. Before the film was completely cured, the prepared AgNW NFs mesh (10 μm) would be attached to both surfaces of the film to form the electrode with semi-embedded surface structure. The perforation distributed on the electrode was developed by Engraving machines laser (Universal PLS6.75, USA).

Fabrication of GW-TENG: The two arched components of GW-TENG were made by 3D printing (SLA 3D printer) with UV Curable Resin (DSM Imagine 8000, produced by Royal DSM, the Netherlands), with radius of 0.68 rad and size of 10 cm (length) \times 2 cm (width), and two longitudinal-extension fixed end (1 cm) for fixing the electrode. The appearance of the arched component was like a door handle. The FEP film (25 μm) with one surface treated by Al coating (300 nm) was attached to the two arched substrates, where the Al coating was attained through magnetron

sputtering (Discovery635, Denton). The film electrode (10 × 2 cm) was fixed at the middle of GW-TENG and thus two TENG units would be fabricated in one device.

Fabrication of the Self-Charging Power Package: The core modules of the energy package included power energy transfer, self-management energy storage, and DC buck conversion. Two polyester-film capacitors (100 V, 50 μF, M.D.L) were connected in parallel to store the micro energy. The model of rectifiers used here was DB207 (ASEMI), and the Al electrolytic capacitor (100 V, YXA) was purchased from Rubycon, Japan. The inductors (PK0608) were purchased from DJS, China, while the resistors were metal film resistors produced by TeleSky, China. The silicon controlled rectifier (SCR) was adopted with PCR606 SOT-23. The whole size of the energy package was 11.5 × 9 × 4.5 cm, while the input end for power source (GW-TENG) and outlet end of the package were reserved.

Characterization and Measurement: Microstructure of the samples was acquired by using SEM (SU8020, Hitachi) and AFM (MFP-3D-SA, Asylum Research). Videos and photographs were captured by camera (Canon 600D, Japan) and high-speed camera (Photron, Japan). Mechanical tensile and stretch cycling tests were operated in an ESM301/Mark-10 system. The strain rate of films during test was around 0.016 per second, and the geometry of these films was rectangle (with tested width of 2.5 cm, length 2–3 cm). The electrical output of the device was measured by Stanford Research Systems Keithley 6514.

Supporting Information

Supporting Information is available from the Wiley Online Library or from the author.

Acknowledgements

Z.R. and Z.W. contributed equally to this work. The research was supported by the National Key R & D Project from Minister of Science and Technology (2016YFA0202704), National Natural Science Foundation of China (Grant Nos. 51605033, 51432005, 5151101243, 51561145021), Beijing Municipal Science & Technology Commission (Z171100000317001, Z171100002017017, Y3993113DF). The authors would like to thank Prof. Tao Jiang and Dr. Kai Han for helpful discussions.

Conflict of Interest

The authors declare no conflict of interest.

Keywords

energy harvesting, light breezes, triboelectric nanogenerators

Received: May 28, 2020

Revised: July 14, 2020

Published online:

- [1] P. Veers, K. Dykes, E. Lantz, *Science* **2019**, 366, 2027.
 [2] E. Rinne, H. Holttinen, J. Kiviluoma, S. Rissanen, *Nat. Energy* **2018**, 3, 494.
 [3] REN21-Renewables 2019 Global Status Report [Online]. Available: <http://www.ren21.net> (accessed: July 2019).
 [4] F. Spinato, P. J. Tavner, G. J. W. Bussell, E. Koutoulakos, *IET Renew. Power Gener.* **2009**, 3, 387.
 [5] D. M. Eggleston, F. Stoddard, *Wind Turbine Engineering Design*, Van Nostrand Reinhold, New York, NY, USA **1987**.

- [6] J. Jonkman, S. Butterfield, W. Musial, G. Scott, *Definition of A 5-MW Reference Wind Turbine for Offshore System Development*, NREL, Golden, CO, USA **2009**.
 [7] E. B. Arnett, *Front. Ecol. Environ.* **2011**, 9, 209.
 [8] A. K. Wright, D. H. Wood, *J. Wind Eng. Ind. Aerod.* **2004**, 92, 1265.
 [9] C. Eisenhut, *IEEE Trans. Energy Convers.* **2007**, 22, 414.
 [10] M. Hampsey, D. H. Wood, *Wind Eng.* **1999**, 23, 31.
 [11] S. Petroni, *RSC Adv.* **2015**, 5, 14047.
 [12] R. Datta, V. T. Ranganathan, S. Member, *IEEE Trans. Energy Convers.* **2002**, 17, 414.
 [13] D. A. Spera, *Wind Turbine Technology*, ASME, Fairfield, NJ, USA **1994**.
 [14] F. Blaabjerg, K. M. Member, *IEEE J. Emerg. Sel. Top. Power Electron.* **2013**, 1, 139.
 [15] P. Gipe, *Wind Eng.* **2004**, 28, 629.
 [16] J. K. Lundquist, K. K. DuVivier, D. Kaffine, J. M. Tomaszewski, *Nat. Energy* **2019**, 4, 26.
 [17] Y. G. Kumar, J. Ringenberg, S. S. Depurua, V. K. Devabhaktuni, J. W. Lee, E. Nikolaidis, B. Andersen, A. Afjeh, *Renewable Sustainable Energy Rev.* **2016**, 53, 209.
 [18] S. Emeis, *Wind Energy Meteorology: Atmospheric Physics for Wind Power Generation*, Springer, Berlin, Germany **2018**.
 [19] F. Fan, Z. Tian, Z. L. Wang, *Nano Energy* **2012**, 1, 328.
 [20] Z. L. Wang, *ACS Nano* **2013**, 7, 9533.
 [21] S. Cui, Y. Zheng, T. Zhang, D. Wang, F. Zhou, W. Liu, *Nano Energy* **2018**, 49, 31.
 [22] H. Yang, M. Deng, Q. Tang, W. He, C. Hu, Y. Xi, R. Liu, Z. L. Wang, *Adv. Energy Mater.* **2019**, 9, 1901149.
 [23] J. Y. Bae, J. Lee, S. M. Kim, J. Ha, B. S. Lee, Y. J. Park, C. Choong, J. B. Kim, Z. L. Wang, H. Y. Kim, J. J. Park, U. I. Chung, *Nat. Commun.* **2014**, 5, 4929.
 [24] Z. Ren, Y. Ding, J. Nie, F. Wang, L. Xu, S. Lin, X. Chen, Z. L. Wang, *ACS Appl. Mater. Interfaces* **2019**, 11, 6143.
 [25] Y. Feng, L. Zhang, Y. Zheng, D. Wang, F. Zhou, W. Liu, *Nano Energy* **2019**, 55, 260.
 [26] L. Zhang, B. B. Zhang, J. Chen, L. Jin, W. Deng, J. Tang, H. Zhang, H. Pan, M. Zhu, W. Yang, Z. L. Wang, *Adv. Mater.* **2016**, 28, 1650.
 [27] Z. C. Quan, C. B. Han, T. Jiang, Z. L. Wang, *Adv. Energy Mater.* **2016**, 6, 1501799.
 [28] A. Ahmed, I. Hassan, P. Song, M. Gamaleldin, A. Radhi, N. Panwar, S. C. Tjin, A. Y. Desoky, D. Sinton, K. T. Yong, J. Zu, *Sci. Rep.* **2017**, 7, 17143.
 [29] J. Hu, X. Pu, H. Yang, Q. Zeng, Q. Tang, D. Zhang, C. Hu, Y. Xi, *Nano Res.* **2019**, 12, 3018.
 [30] Y. Xie, S. Wang, L. Lin, Q. Jing, Z. H. Lin, S. Niu, Z. Wu, Z. L. Wang, *ACS Nano* **2013**, 7, 7119.
 [31] M. L. Seol, J. H. Woo, S. B. Jeon, D. Kim, S. J. Park, J. Hur, Y. K. Choi, *Nano Energy* **2015**, 14, 201.
 [32] Z. Zhao, X. Pu, C. Du, L. Li, C. Jiang, W. Hu, Z. L. Wang, *ACS Nano* **2016**, 10, 1780.
 [33] Y. Xi, H. Guo, Y. Zi, X. Li, J. Wang, J. Deng, S. Li, C. Hu, X. Cao, Z. L. Wang, *Adv. Energy Mater.* **2017**, 7, 1602397.
 [34] J. H. Zhang, Y. Li, J. H. Du, X. H. Hao, H. T. Hua, *J. Mater. Chem. A* **2019**, 7, 11724.
 [35] L. C. Caldas, M. Behn, U. Tapken, DAGA, Rostock, Deutschland **2019**.
 [36] S. Niu, S. Wang, L. Lin, Y. Liu, Y. Zhou, Y. Hua, Z. L. Wang, *Energy Environ. Sci.* **2013**, 6, 3576.
 [37] Y. Zi, H. Guo, Z. Wen, M. H. Yeh, C. Hu, Z. L. Wang, *ACS Nano* **2016**, 10, 4797.
 [38] Y. Zi, S. Niu, J. Wang, Z. Wen, W. Tang, Z. L. Wang, *Nat. Commun.* **2015**, 6, 8376.
 [39] F. Xi, Y. Pang, W. Li, T. Jiang, L. Zhang, T. Guo, G. Liu, C. Zhang, Z. L. Wang, *Nano Energy* **2017**, 37, 168.
 [40] H. Qin, G. Cheng, Y. Zi, G. Gu, B. Zhang, W. Shang, F. Yang, J. Yang, Z. Du, Z. L. Wang, *Adv. Funct. Mater.* **2018**, 28, 1805216.